Ceramics International xxx (xxxx) xxx–xxx

Contents lists available at ScienceDirect

Ceramics International

journal homepage: www.elsevier.com/locate/ceramint

Visible light enhanced black NiO sensors for ppb-level NO_2 detection at room temperature

Xin Geng[a,b], Driss Lahem[c], Chao Zhang[a,*], Chang-Jiu Li[d,*], Marie-Georges Olivier[b], Marc Debliquy[b]

[a] College of Mechanical Engineering, Yangzhou University, Yangzhou 225127, PR China
[b] Service de Science des Matériaux, Faculté Polytechnique, Université de Mons, Mons 7000, Belgium
[c] Material Science Department, Materia Nova ASBL, Mons 7000, Belgium
[d] State Key Laboratory for Mechanical Behavior of Materials, Xi'an Jiaotong University, Xian 700149, PR China

ARTICLE INFO

Keywords:
NiO
NO_2 sensor
Room temperature
Visible light irradiation

ABSTRACT

Although extensive studies have been carried out on n-type semiconductors for room-temperature gas sensor applications, some intrinsic problems remain. Therefore, other interesting attempts should be adopted to solve these issues, like p-type semiconductors. Previous studies have demonstrated that p-type semiconductor gas sensors exhibit better selectivity and less humidity dependence due to the distinctive oxygen adsorption and surface reactivity. Visible light is used as the external activation source to accelerate the sensing kinetics instead of heating. Stoichiometric NiO cannot absorb visible lights. Inspired by the works of black TiO_2, we adopted three methods to prepare black NiO. XPS characterizations reveal that the presence of Ni^{3+} ions leads to the formation of black NiO. However, not all black NiO samples show good responses to NO_2 at room temperature. Three main routes: synthesizing specific morphology with large specific surface area and porosity, introduction of Ni^{3+} ions and oxygen vacancies, are needed to get the enhanced sensing performance. The black NiO samples with large specific surface area and oxygen vacancies and Ni^{3+} ions show obvious response towards ppb-level NO_2 with visible light irradiation at room temperature. Furthermore, light wavelength is found to play a vital role in the sensing characteristics, and blue light is the optimal choice. Different from traditional NiO sensors operated at high temperatures exhibiting superior response to reducing gases, the black NiO show excellent selectivity towards oxidizing gas, ppb-level NO_2, at room temperature illuminated by blue light. In contrast with n-type semiconductors, the black NiO samples also exhibit less humidity dependence.

1. Introduction

In the past decades, semiconductor gas sensors have attracted considerable attention as a result of many advantages, such as high sensitivity, low cost, easy integration, etc [1–3]. Most efforts were focused on the n-type semiconductors for gas sensor applications, such as SnO_2, ZnO, WO_3, In_2O_3, TiO_2, etc [4–8]. More than 90% publications were concentrated on the research of the gas sensors fabricated by n-type semiconductors [9]. However, till now, some problems of n-type semiconductor gas sensors still exist that is difficult to be solved, like the selectivity and humidity dependence. As a consequence, other attempts should be made to investigate other semiconductor materials for providing new gas sensors with enhanced sensing performance. Kim and Lee [9] supposed that p-type semiconductors were good candidates for fabricating highly sensitive gas sensors, which has many merits, such as better selectivity, less sensitive to humidity, and enhanced recovery rate. Among the p-type semiconductors, NiO is the most promising material and has received widespread attention, due to its availability, nontoxicity, chemical and biological stability.

Traditional NiO gas sensors are operated at elevated temperatures ranging from 200 °C to 600 °C to obtain acceptable gas sensing properties. At high temperatures, NiO based gas sensors have been reported to be good candidates for detecting reducing gases, like H_2, NH_3, HCHO, xylene, toluene, acetone, etc [10–17]. For instance, Turgut et al. reported that the pristine NiO film deposited by RF sputtering showed good response to ppm-level H_2 at 600 °C [10]. As well known, morphology plays a vital role in selectivity, Li found that the NiO nanowires exhibited remarkable selectivity to HCHO at 200 °C [11]. Apart from adjusting morphology, doping is also a good route to tune selectivity. For example, Lahem et al. reported the strong influence of NiO

* Corresponding authors.
E-mail addresses: zhangc@yzu.edu.cn (C. Zhang), licj@mail.xjtu.edu.cn (C.-J. Li).

https://doi.org/10.1016/j.ceramint.2018.11.097
Received 16 August 2018; Received in revised form 12 November 2018; Accepted 13 November 2018
0272-8842/ © 2018 Elsevier Ltd and Techna Group S.r.l. All rights reserved.

synthesis routes on the gas sensing performance towards ppb-level of formaldehyde [16]. Gao et al. demonstrated that hierarchical Sn-doped NiO synthesized by a hydrothermal method displayed superior response towards ppm-level xylene at 300 °C [12]. In addition, noble metal sensitization also can be used to manipulate the sensing behaviors. Chen et al. found that the Pt-NiO prepared by RF sputtering was significantly sensitive to ppb-level NH_3 at 300 °C [13].

However, high-temperature semiconductor gas sensors are facing many issues, such as high power-consumption, thermally-induced grain growth, detection risks in inflammable and explosive gases [18]. The sintering and diffusion effect at the grain boundaries at high temperatures will result in grain growth, which adversely affects the long-term stability [19]. In addition, high working temperature also requires special substrates that can withstand high temperature, normally using rigid substrates like ceramics and eliminating the use of flexible substrates, which increases the design complexity and operating cost. Therefore, it is imperative to fabricate room-temperature gas sensors. To the best of our knowledge, room-temperature NiO gas sensors are seldom reported so far. Nevertheless, previous studies are found that the sensing behaviors of metal oxides are very poor at room temperature, especially the response and recovery speed [20,21]. Consequently, other external excitation energies instead of heating are desired to accelerate the reaction kinetics. Adopting light irradiation is a feasible method to enhance the response and recovery kinetics process [22,23]. However, the wide bandgap of NiO of 3.6–4.0 eV (depending on the synthesis method and crystallinity) does not allow to use cheap LED's working in the visible range, so efficient strategies should be adopted to extend the light absorption range. Enlightened by the black TiO_2 which effectively widens the light absorbing range, black NiO may be a good solution to enlarge the light absorption region [24].

Furthermore, surface states play an important role in the sensing performance [25]. There are six types of predominant defects, i.e., metal interstitial, metal vacancy, metal antisite, oxygen interstitial, oxygen vacancy, and oxygen antisite [26]. Metal interstitial and oxygen vacancy are donor defects, while metal vacancy and oxygen interstitial are acceptor defects. Oxygen vacancies can remarkedly enhance the surface reactivity, and are said to be preferential sites for oxidizing gases, which in turn improve the selectivity of metal oxides [21–23,27]. As a result, incorporating oxygen vacancies into NiO may enhance its selectivity towards oxidizing gases.

Besides, morphology also has a crucial influence on the sensing performance, involving sensitivity, selectivity, etc [2,3,8]. Adjusting morphologies mainly affect two factors, including specific surface area and exposed facets. Increasing specific surface area can greatly increase the adsorption site numbers. The surface reactivity is highly associated with facets according to the simulation and experimental results [28]. So synthesizing metal oxides with exposed facets favoring the reaction and large specific surface area is a good route to improve the sensing performance.

In this study, two synthesis methods, i.e., precipitation, and a hydrothermal method, have been used to prepare black NiO with rich oxygen vacancies and well-defined morphologies. XRD, XPS and UV–Vis techniques were used to characterize the samples and found that the reason for black color of those samples is the presence of Ni^{3+} ions. In addition, the presence of abundant Ni^{3+} ions and oxygen vacancies have positive effects on the sensing performance. The NiO samples with well-defined morphology, rich Ni^{3+} ions or highly concentrated oxygen vacancies exhibit a remarkable response to ppb-level NO_2 at room temperature with visible light irradiation. Different from the NiO sensors at high temperatures, the samples prepared in this study has no response to reducing gases at room temperature, which exhibits a better selectivity. Therefore, this study provides a new way to prepare room-temperature gas sensors with enhanced sensing performance using p-type semiconductors.

2. Experimental method

2.1. Synthesis of NiO samples

Three kinds of NiO samples were synthesized by different methods, hydrothermal method from nickel nitrate, and two precipitation methods from nickel malonate and nickel sulfate precursors.

2.1.1. Synthesis of Sample 1 (abbreviated as S1)

S1 was prepared by a hydrothermal method. 0.7 g $Ni(NO_3)_2{\cdot}6H_2O$ and 0.5 g Polyethylene glycol 6000 (PEG 6000) are dissolved in 45 mL of DI water under vigorous stirring at room temperature. Subsequently, 2.5 mL triethylamine $N(C_2H_5)_3$ is added to the above system dropwise and stirred for 50 min. The obtained mixture is then transferred into a Teflon-lined stainless steel autoclave, and maintained at 140 °C for 12 h. After cooling to room temperature naturally, the product is filtered, washed several times with distilled water and ethanol for several times, and dried in vacuum at 80 °C for 12 h. Finally, the synthesized powders were calcined at 400 °C for one hour.

2.1.2. Synthesis of Sample 2 (abbreviated as S2)

S2 was prepared by a precipitation method from nickel malonate ($(CH_3CH_2COO)_2Ni$). The malonate ligand is used as the precipitating agent to synthesize NiO. Ten mmol lithium hydroxide was added to 5 mmol malonic acid until the pH was adjusted to 7. Afterward, the nickel chloride aqueous solution was added to the above solution dropwise with continuous stirring at 90 °C for 3 h under reflux. Subsequently, the precipitate was filtered and washed with DI water, isopropanol and acetone, respectively. The product was dried at 70–80 °C, and then calcined at 500 °C to obtain the final sample.

2.1.3. Synthesis of Sample 3 (abbreviated as S3)

S3 was prepared by the precipitation method from nickel sulfate ($NiSO_4$). 5.2 mmol nickel sulfate was first dissolved in 80 mL DI water. After that, 0.083 mol urea was added to the above solution, and the mixture solution put at 80 °C for 4 h. The product was filtered, washed with DI water and absolute ethanol several times. Finally, the synthetized powders were dried, and calcined at 400 °C for one hour.

2.2. Sample characterization

The crystal structure and phase constitutions of the NiO samples where determined by Multi-Functional X-ray Diffractometer (XRD, D8 Advance, Bruker AXS, Germany). The detailed information of elemental valence for all the samples was acquired by X-ray photoelectron spectroscopy (XPS, ESCALAB 250Xi, Thermo Scientific, USA). Field-emission scanning electron microscopy (FE-SEM, S4800II, Hitachi, Japan) was used to observe the surface morphology. UV–Vis diffuse reflectance spectrophotometer (Cary5000, Varian, USA) was utilized to record the light absorption properties of all the NiO samples.

2.3. Sensor preparation and gas sensing test

The prepared NiO powders were mixed with terpineol to form a homogenous paste, and then the paste was screen printed on the commercial alumina sensor substrates (C-MAC Micro Technology Company, Belgium). Afterward, the sensor was dried at 70 °C, and then heated at 400 °C to remove the terpineol. The gas sensing tests were performed in a home-made gas sensing measuring system. LED lamps with different wavelengths were installed in front of the NiO sensors. The details can be found in [20–23].

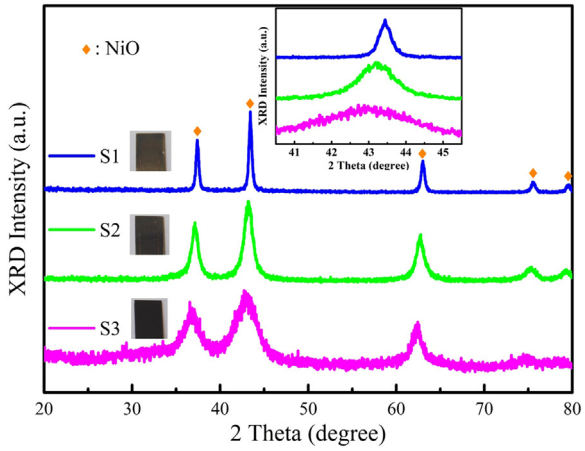

Fig. 1. X-ray diffraction patterns of the black NiO samples (insert: the photos of the black samples).

3. Results and discussion

3.1. Sample characterization and gas sensing tests

Normally, the color of stoichiometric NiO is green. However, all the samples prepared in this study are black (the insert in Fig. 1). Detailed characterization was performed in order to identify the phase constitution and structure of the NiO samples. Fig. 1 shows the XRD pattern of all the samples in the range of 20–80°. Five obvious diffraction peaks situated at 37.16°, 43.27°, 62.50°, 75.08° and 79.17° are clearly observed for all samples. These peaks respectively correspond to (111), (200), (220), (311) and (222) crystal planes of NiO with face-centered cubic structure (JCPDS 78-0428) [29]. It is interesting to notice that the (200) plane of S1, S2 and S3 are respectively located at 43.26°, 43.22°, and 42.88°, indicating that there is angle shift in the as-prepared samples. The phenomenon of angle shift maybe attributed to the surface defects, which needs other technique to confirm, such as XPS.

XRD results just can offer the phase composition and crystal structure, however, they cannot provide more information about the valence states of elements. XPS is such a technique that can gain more insights of the elements of Ni and O. The binding energies were calibrated by C1s at 284.6 eV, and the Shirley background was subtracted from the XPS spectra. Fig. 2 depicts the surface core level spectra of Ni2p and O1s. The Ni2p core level spectra of all samples are similar, as shown in Fig. 2(a). Ni2p orbital has shown four peaks situated at ca. 855 eV, 861.3 eV, 872.8 eV and 879.1 eV assigned to $Ni2p_{3/2}$, $Ni2p_{3/2}$ satellite, $Ni2p_{1/2}$ and $Ni2p_{1/2}$ satellite [10]. It is worth noting that the $Ni2p_{3/2}$ spectrum is overlapped by two shoulders of 853.5 eV and 855.5 eV corresponding to Ni^{2+} (N_2) and Ni^{3+} (N_3), respectively [30]. As a consequence, the intensity ratio of $N_3(I_{N3})$ and $N_2(I_{N2})$ can reflect the relative content of Ni^{3+} in NiO samples. The intensity ratio (I_{N3}/I_{N2}) is respectively 0.964, 0.909, and 0.985 for S1, S2 and S3, indicating all the samples involve Ni^{3+} ions, and the amount of Ni^{3+} ions is in the sequence of S3, S1, and S2. Inspired by the hydrogenated black TiO_2, introducing Ti^{3+} into TiO_2 causes its color turns from white to black [24]. The color change of NiO in this study also can be attributed to the incorporation of Ni^{3+} ions. Fig. 2(b) shows the high-resolution spectra of O1s, which exhibits a doublet shoulder at energies of 529.1 eV and 531.1 eV (respectively abbreviated as O_a and O_b) [21–23]. The formation of O_a peak is attributed to the lattice oxygen of stoichiometric nickel oxides, while O_b is ascribed to oxygen vacancies. Similar to Ni element, the intensity ratio of O_b and O_a (I_{Ob}/I_{Oa}) also can directly reflect the oxygen vacancy concentration. The ratio (I_{Ob}/I_{Oa}) of S1, S2 and S3 is respectively 1.038, 0.807 and 0.656, indicating S1 has the highest oxygen vacancy concentration. Combined with XRD and XPS results, it can be inferred that S3 has largest amount of Ni^{3+}, while S1 possess the highest oxygen vacancy concentration.

Apart from chemical compositions, morphology is well known to play a vital role in the sensing performance. Fig. 3 shows the FE-SEM images of all the samples with the same magnification. S1 exhibits a well-defined morphology of hexagonal nanodisks with size ca. 30 nm. S2 shows a layered structure accumulated by spherical nanosized grains with size ca. 25 nm, and S3 is also a layered structure made of nanosheets with size ca. 30 nm. In addition, S2 and S3 are far less porous than S1. The porous structure can provide more adsorption sites and gas diffusion channels, which is beneficial to improve the gas sensing characteristics.

The target in this work is to develop room-temperature NO_2 gas sensors, so all the samples are tested at room temperature, as shown in Fig. 4. It can be observed that all the samples exhibit almost no response to 5 ppm NO_2 at room temperature in the dark. Our previous studies also found similar phenomena for other n-type semiconductors [20–23]. For instance, the sensing properties of ZnO and WO_3 towards ppm-level NO_2 are very poor. In order to get a response, the surface has to be "activated" by bringing energy to make the surface reactions happen. The mechanisms will be detailed in the following section. Usually, metal oxides are activated by heat and work at high temperature (typically in the range of 150–350 °C). Here, light is the source of energy and the effect of the light activation will be studied for these three samples.

Accordingly, light absorption range of the sensitive materials is very essential for light-activated gas sensors. However, the band gap of stoichiometric NiO is ca. 3.6 eV. Thus, in principle, stoichiometric NiO

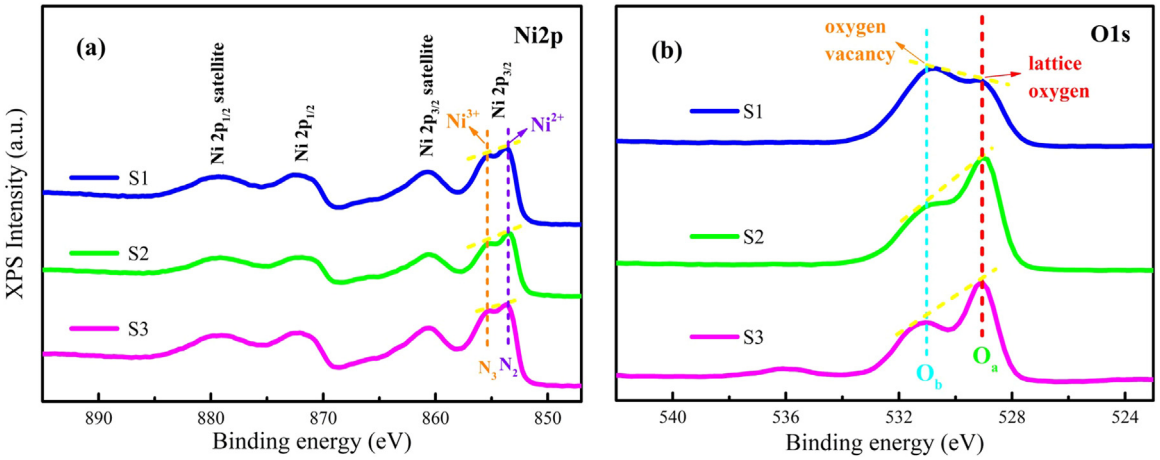

Fig. 2. XPS spectra of the black NiO samples of (a) Ni2p (b) O1s.

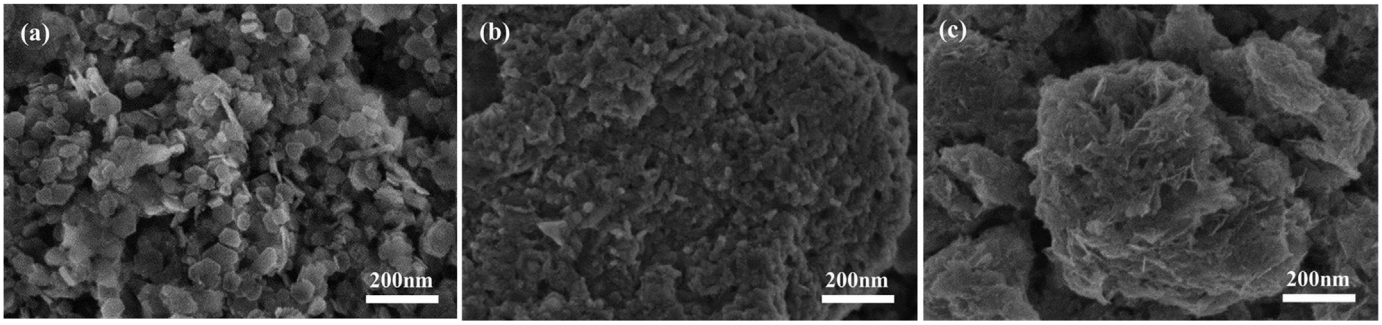

Fig. 3. FE-SEM images of the black NiO samples of (a) S1 (b) S2 (c) S3.

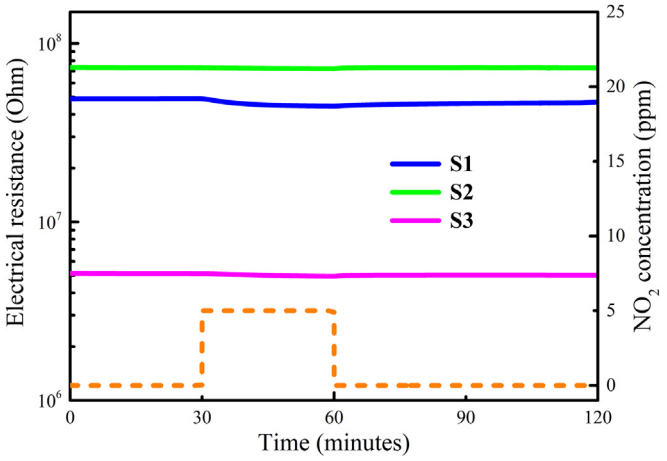

Fig. 4. Sensing resistance of the black NiO samples to 5 ppm NO_2 at room temperature in the dark.

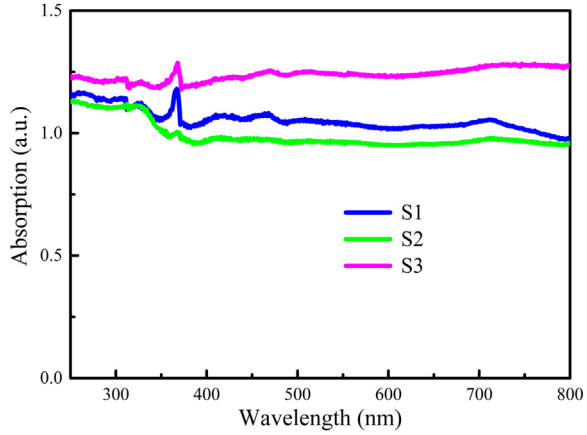

Fig. 5. UV–Vis spectra of the black NiO samples.

just can absorb light with wavelength less than 354 nm and 337 nm. Fig. 5 illustrates the UV–Vis spectra of all samples at the wavelength ranging from 250 nm to 800 nm. It can be observed that all the samples absorb in the whole visible and UV region. The light absorption intensity of all samples is in the sequence of S3, S1 and S2, which is well in line with the amount of Ni^{3+} ions. The color of Ni_2O_3 is known to be black, and that of NiO is green. As observed in the XPS spectra, all the samples contain Ni^{3+}, which turns the color of the samples from green to black, and extends to the whole visible spectrum. The light absorption range of NiO is increases monotonously with Ni^{3+} ion concentration.

As well known, the photon energy depends on the light wavelength according to the equation: $E = hc/\lambda$. So, it is necessary to study the effect of light wavelength on the sensing performance. Fig. 6 plots the response of all samples towards 372 ppb NO_2 with visible light irradiation of different wavelength. Relevant results, like sensitivity, response time, and recovery time are summarized in Tables 1–3. From the testing results above, several conclusions can be drawn.

First, even under the same light illumination, all samples have different base resistance, and follow in the sequence of S2, S1, S3. The resistance of S1 and S2 is almost the same, while that of S3 is much lower, which is two orders of magnitude smaller, which is contrary to the UV–Vis spectra results. The more photon energy absorbed by the materials, the more carriers are generated, which leads to lower base resistance.

Second, the sensing performance of S1 is much better than S2 and S3. S2 and S3 almost exhibit no response to ppb-level NO_2, while S1 shows obvious response to 372 ppb NO_2 with visible light irradiation at room temperature in terms of sensitivity, response time and recovery time. For example, the sensitivity for S1, S2, S3 under blue light activation are respectively 31.04%, 1.89%, and 5.22%. Besides, the response time of S1 is 13.2 min, while the counterparts of S2 and S3 are very slow more than 30 min. The reason for the improved performance of S1 is predominantly attributed to well-defined morphology, large specific surface area, a high concentration of Ni^{3+} ions and oxygen vacancy. The morphology of hexagonal nanodisks is said to enhance the surface activity [31], which can greatly accelerate the surface reactivity process. According to the XPS spectra, S1 has the highest oxygen vacancy concentration and second highest concentration of Ni^{3+} ions. Oxygen vacancies are reported to be preferential adsorption sites for NO_2 molecules, so large concentrations of oxygen vacancies can significantly increase the adsorption site density and improve the sensing properties. Based on [32], incorporating Ni^{3+} into NiO can remarkedly enhance the sensing characteristics due to the synergistic effect between Ni^{2+} and Ni^{3+}, which can facilitate and promote the adsorption behaviors of acceptor gases on NiO. As a consequence, the black NiO just enable the visible light absorption, however, not all the black NiO possess excellent room-temperature NO_2 sensing properties with visible light irradiation. Other parameters, including rich oxygen vacancies, special morphology, and large specific surface area are required to improve the room-temperature NO_2 sensing properties of black NiO with visible light stimulation at room temperature.

Third, light wavelength plays a crucial role in the sensing performance. In order to analyze and describe the effect of light wavelength clearly, the data of S1 is selected and shown in Fig. 7, and Table 4. As S2 and S3 give no response, they were not further studied. It can be observed that the base resistance decreases when the wavelength reduces from red to purple light. Furthermore, the sensitivities, response time, and recovery time are reduced with the decrease in wavelength. For instance, the sensitivities of S1 are respectively 88.94%, 53.33%, 31.04%, and 24.21% ranging from red to purple light. The response time is respectively 20.8 min, 17.6 min, 13.2 min, and 14.1 min. It is worth to note that the response and recovery time obtained by the blue light is shorter than that of purple light. Similar results are also found

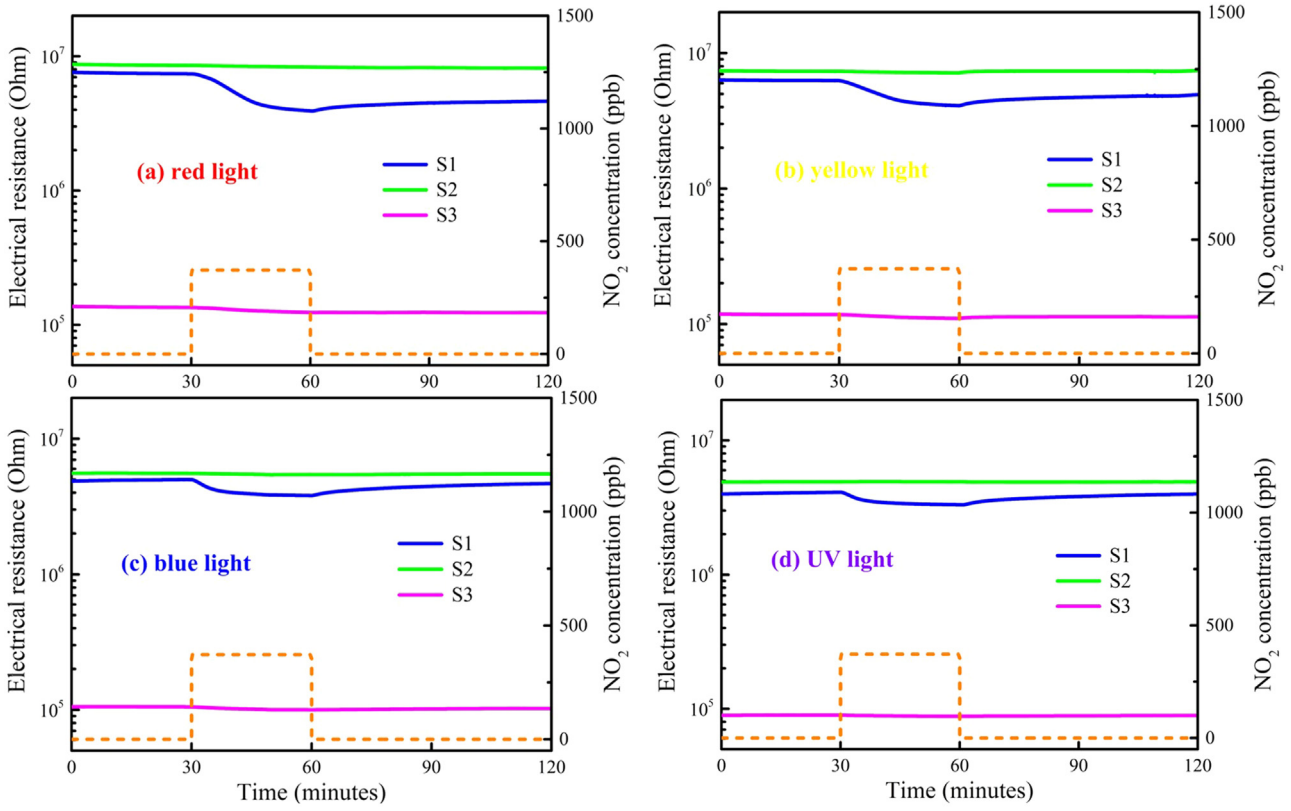

Fig. 6. Electrical resistance of the black NiO samples versus 372 ppb NO_2 illuminated by visible lights with different wavelengths at room temperature.

Table 1
Sensor response ($(R_{air}/R_{NO2}-1)\times100\%$) of the black NiO samples to 372 ppb NO_2 under visible light illumination with different wavelengths at room temperature.

Samples	Red light	Yellow light	Blue light	UV light
S1	88.94%	53.33%	31.04%	24.21%
S2	2.99%	2.85%	1.89%	1.01%
S3	9.24%	6.84%	5.22%	2.03%

Table 2
Response time (minutes) of the black NiO samples to 372 ppb NO_2 under visible light illumination with different wavelengths at room temperature.

Samples	Red light	Yellow light	Blue light	UV light
S1	20.8	17.6	13.2	14.1
S2	> 30	> 30	> 30	> 30
S3	> 30	> 30	> 30	> 30

Table 3
Recovery time (minutes) of the black NiO samples to 372 ppb NO_2 under visible light illumination with different wavelengths at room temperature.

Samples	Red light	Yellow light	Blue light	UV light
S1	> 60	> 60	29.1	31.7
S2	> 60	> 60	> 60	> 60
S3	> 60	> 60	> 60	> 60

for WO_3 [33] and ZnO [20–23]. Moreover, additional reactions are taken place with purple light stimulation via:

$$NO_2 + h\nu \rightleftharpoons NO + O \quad (1)$$

$$O_2 + O \rightleftharpoons O_3 \quad (2)$$

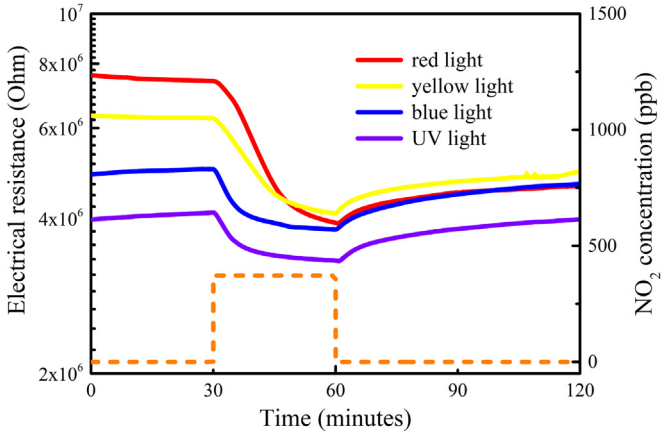

Fig. 7. Sensing behaviors of S1 towards 372 ppb NO_2 with visible light activation of different wavelengths at room temperature.

$$NO + O_3 \rightleftharpoons NO_2 + O_2 \quad (3)$$

These reactions would reduce the adsorption and desorption rate of NO_2^- species, which slows down the response and recovery process. As a consequence, blue light is the optimal source to achieve the best sensing performance at room temperature.

Fig. 8 displays the electrical resistance of all samples versus the NO_2 concentration of 57 ppb, 180 ppb, and 372 ppb with blue light illumination at room temperature. The analyzed results are listed in Table 5. S1 shows obvious response towards 57 ppb, 180 ppb, and 372 ppb NO_2 activated by blue light at room temperature. The detection limit is as low as 57 ppb. Besides, the sensor response increases linearly with NO_2 concentration, as shown in the insert of Fig. 8.

For room temperature gas sensors, it is well known that humidity variations can have a big impact on metal oxide sensors. So, it is

Table 4
Sensing characteristics of S1 to 372 ppb NO_2 under visible light illumination with different wavelengths.

Wavelength (nm)	Light color	R_{air} (Ω)	Sensor response (R_{air}/R_{NO2}-1)×100%	Response time (min)	Recovery time (min)
640	Red	7.41×10^6	88.94%	20.8	> 60
580	Yellow	6.26×10^6	53.33%	17.6	> 60
480	Blue	4.99×10^6	31.04%	13.2	29.1
380	UV	4.11×10^6	24.21%	14.1	31.7

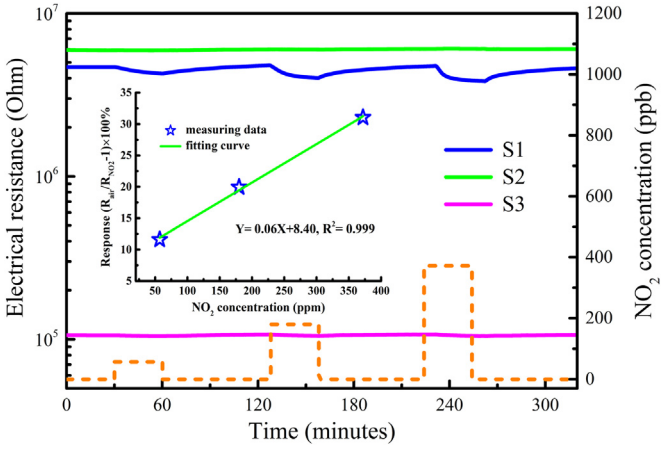

Fig. 8. Electrical resistance of the black NiO samples to 57 ppb, 180 ppb, and 372 ppb NO_2 with blue light irradiation at room temperature, insert: the fitting curve of response and NO_2 concentration. (For interpretation of the references to color in this figure legend, the reader is referred to the web version of this article.)

Table 5
Sensor response ((R_{air}/R_{NO2}-1)×100%) of the black NiO samples to 57, 180 and 372 ppb NO_2 with blue light illumination at room temperature.

Samples	57 ppb	180 ppb	372 ppb
S1	11.60%	19.94%	31.04%
S2	0.37%	1.26%	1.89%
S3	1.89%	3.51%	5.22%

important to follow the influence of humidity on the resistance of the sensors. In contrast with n-type ones, p-type semiconductors are said to be less moisture sensitive, Fig. 9(a) shows the effect of humidity on the electrical resistance of all the samples, and relevant results are

Table 6
Effect of humidity on the base resistance of the black NiO samples with blue light illumination at room temperature.

Samples	0% (Ohm)	100% (Ohm)
S1	4.92×10^6	1.25×10^6
S2	5.57×10^6	3.26×10^6
S3	1.05×10^5	6.74×10^4

summarized in Table 6. The resistance of n-type semiconductors always decreases with the humidity increasing. Different with n-type ones, the resistance of p-type ones, especially S1, increases in the initial stage and then reduces with further increasing humidity. For instance, the resistance of S1 increases when humidity changes from 0% to 10%, as the humidity further increasing, the resistance decreases. When humidity is low, water molecules will dissociate into hydroxyl, and give electrons to NiO. The produced electrons would recombine with holes, increasing the resistance according to the equation below:

$$2H_2O + O_2^- \rightleftharpoons 4OH + e^- \quad (4)$$

$$e^- + h^+ \rightleftharpoons \text{null} \quad (5)$$

Besides, water molecules occupy part of the adsorption sites, so less oxygen species adsorb on the surface, which also decreases the hole concentration and increases resistance. When humidity further increases, Grotthuss mechanism (also known as proton hopping) dominates the reaction process, which reduces the resistance via:

$$H_2O + H^+ \rightleftharpoons H_3O^+ \quad (6)$$

In addition, the resistance variation is highly associated with the samples. Those samples which exhibit remarkable response to NO_2 gas, like S1, are also sensitive to water molecules. The resistance of S1 reduces by two-thirds. Nevertheless, S2 and S3 are less sensitive to not only NO_2 gas, but also humidity. This allows us to conclude that the morphology of these samples is not favorable for gas adsorption and gas

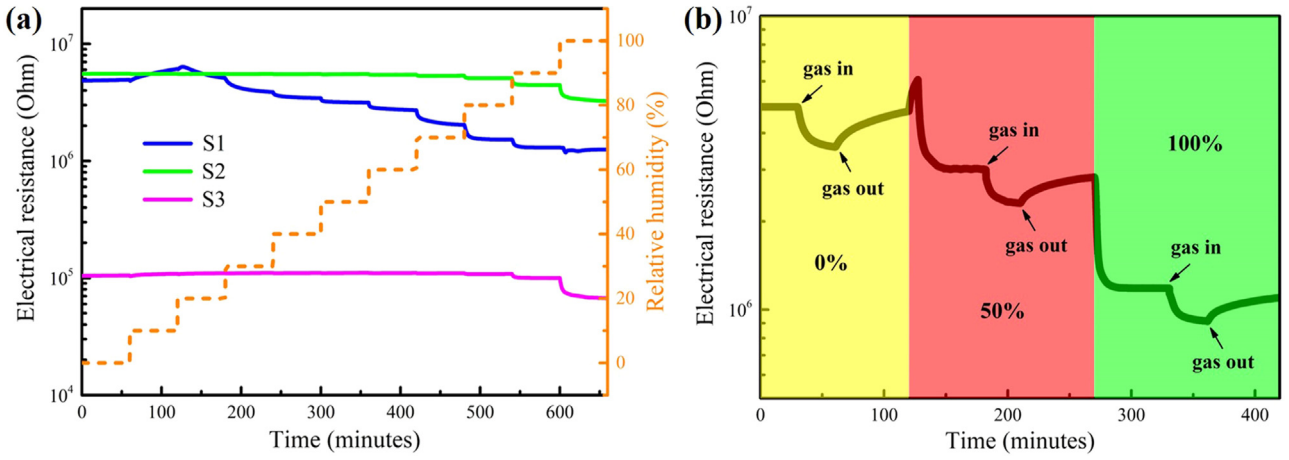

Fig. 9. (a) Effect of humidity on the base resistance of the black NiO samples; (b) Electrical resistance responses of S1 to 372 ppb NO_2 with relative humidity of 0%, 50% and 100% under blue light irradiation at room temperature. (For interpretation of the references to color in this figure legend, the reader is referred to the web version of this article.)

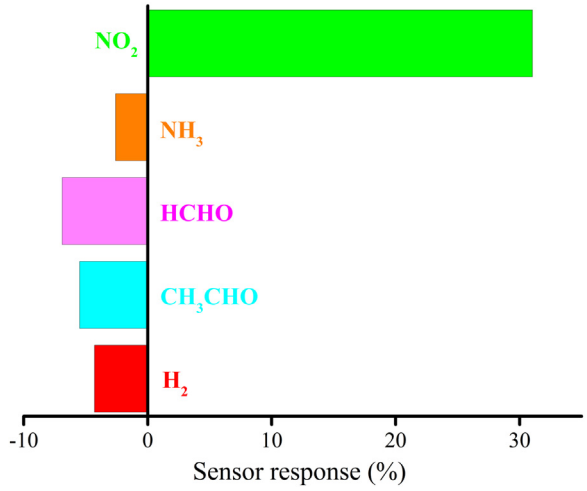

Fig. 10. Selectivity of S1 towards 372 ppb NO_2, 5 ppm NH_3, 5 ppm HCHO, 5 ppm CH3CHO, and 1000 ppm H_2 irradiated by blue light at room temperature.

response. Compared with the influence of humidity on resistance of n-type semiconductors, for example, ZnO is often used as the humidity sensor application [34,35], humidity has a much smaller effect on resistance of the samples prepared in this study. Fig. 9(b) illustrates the gas response of S1 towards 372 ppb NO_2 with relative humidity of 0%, 50% and 100% under blue light illumination at room temperature. S2 and S3 almost exhibit no response to 372 ppb NO_2, which are not shown herein. The trend of electrical resistance variation is consistent with Fig. 9(a). Besides, the sensitivity decreases with humidity increasing. When humidity changes from 0%, 50% to 100%, the sensitivities are respectively 36.6%, 31.04% and 29.8%. When humidity increases from 0% to 100%, the sensitivity decreases 18.6%. Therefore, humidity has a negative effect on the NO_2 sensing response, which leads to a lower sensitivity. The reduction of gas response should be attributed to the decrease of adsorption sites occupied by water molecules.

Traditionally, selectivity is an important issue for metal oxide gas sensors [36]. Fig. 10 illustrates the gas sensing response of S1 towards several kinds of interfering gases apart from NO_2, such as 5 ppm NH_3, 5 ppm HCHO, 5 ppm CH_3CHO, and 1000 ppm H_2, with blue light illumination at room temperature. It can be found that the response of S1 to NO_2 is at least four times higher than those towards other gases. As a consequence, the prepared NiO sensors show good selectivity to ppb-level NO_2 irradiated by blue light at room temperature.

3.2. Gas sensing mechanism

As a typical p-type semiconductor, the gas sensing mechanism of NiO is completely different from n-type semiconductors. Hole is the majority carrier, and the electrical resistance of NiO is positively correlated to the hole concentration. The adsorption of acceptor gases, like O_2 and NO_2, will increase the hole concentration and thus reduce the electrical resistance. When NiO samples are exposed in air, O_2 molecules would adsorb on the surface and form O_2^- species by taking electrons from the surface via:

$$O_2 + e^- \rightleftharpoons O_2^- \quad (7)$$

Then, a hole accumulation layer (HAL) region is created near the surface, as depicted in Fig. 11(a). The HAL layer at the shell has low resistance, while the core region is highly resistive, so conduction predominantly takes place along the near-surface HAL region. However, if the bulk conductivity is high (large sub-stoichiometry or large grain), the surface effect becomes negligible.

Considering the wide bandgap of nickel oxide, the generation of charge carriers in the dark at room temperature for intrinsic NiO is very small. To get electron exchanges between the gas and the strong semiconductor interaction are needed, involving as a consequence, chemisorption of the species. At room temperature, the adsorption-desorption phenomena dealing with chemisorption are usually slow energy has to be brought. Moreover, in the case of p-type semiconductors, the adsorption of oxidizing gases is not favored because holes are the majority carriers and the adsorbed species must extract the electron from the valence band (the conduction band is almost empty). Even high concentrations of acceptor gases are injected and adsorbed on the surface, a small part of injected gases can extract electrons from the surface to create a small number of chemisorbed species, which finally leads to a low sensitivity. Therefore, the sensing properties of stoichiometric NiO is supposed to be very bad due to the very low electron concentration. Consequently, external excitation energies, like light illumination, are required to activate NiO to generate more electrons that can participate in the surface reactions. On account of the incorporation of Ni^{3+} ions, the prepared black NiO samples can absorb all the photon energies of visible lights. Upon illumination with visible light, electron-hole pairs are formed. The generated electrons can be more easily captured by adsorbed oxidizing gases. In air, O_2^- species can be chemisorbed on the surface by taking electrons, which increases the thickness of HAL layer (Fig. 11(b)). When NO_2 is injected, NO_2 molecules will occupy the free adsorption sites to capture electrons to create NO_2^- species to further increase the thickness of HAL region through, as displayed in Fig. 11(c):

$$NO_2 + e^- \rightleftharpoons NO_2^- \quad (8)$$

It increases the thickness of conductive region, and in turn decreases the electrical resistance. Consequently, light illumination has a double effect, it speeds up the reactions and increases the amount of adsorbed NO_2 molecules.

Besides, theoretical calculations and sensing experiments have demonstrated that oxygen vacancies can enhance the surface reactivity, and are preferential sites for oxidizing gases [37,38]. Zeng et al. found that the presence of oxygen vacancies would decrease the adsorption energy, increase the electron transfer between ZnO and NO_2 using DFT calculation. Qin et al., also found a similar phenomenon for WO_3 towards NO_2. The interactions between oxygen vacancy sites and NO_2 happen via:

$$V_o^x + NO_2 \rightleftharpoons V_o^{\bullet} + NO_2^- \quad (9)$$

$$V_o^{\bullet} + NO_2 \rightleftharpoons V_o^{\bullet\bullet} + NO_2^- \quad (10)$$

The binding force between oxygen vacancy sites and NO_2 gas molecules are stronger than that of perfect surface and gas molecules. It further widens the HAL layer and decreases the resistance, which results in a higher sensitivity.

4. Conclusions

Three synthesis methods were used to prepare black NiO samples to extend the visible light absorption range due to wide bandgap. Semiconductor of NiO absorbs only UV lights. The NiO samples exhibit a color of black owing to the presence of high concentrations of Ni^{3+} ions, and UV–Vis absorption spectra show that all the black NiO samples have strong absorption in the whole visible light region. The black NiO samples with special morphology, large specific surface area, abundant Ni^{3+} ions and rich oxygen vacancies exhibit good response towards ppb-level NO_2 activated by visible lights at room temperature. The detection limit of the samples towards NO_2 is as low as 57 ppb. The sample synthesized by hydrothermal method using nickel nitrate as the precursor possess highly concentrated oxygen vacancies, and shows a well-defined morphology of hexagonal nanodisks with larger specific surface area and porosity. The incorporation of abundant Ni^{3+} ions and oxygen vacancies, as well as specific morphology and large specific

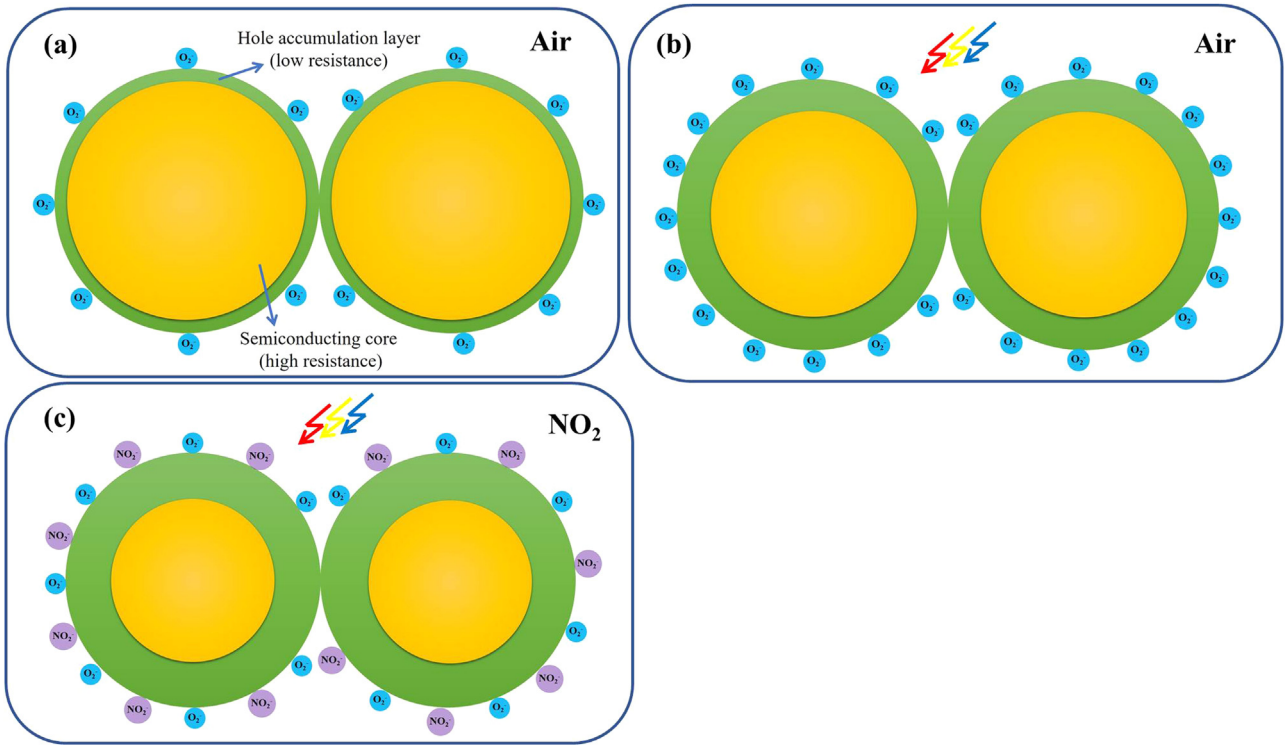

Fig. 11. Schematic of the gas sensing mechanism of the black NiO samples.

surface area contribute to excellent room-temperature NO_2 gas sensing performance with visible light stimulation. In addition, light wavelength also plays an important role in the sensing properties, in terms of base resistance, response and recovery speed. The black NiO samples show less humidity dependence and are better selectivity towards NO_2 gas compared with n-type semiconductors.

Acknowledgments

This work is supported by State Key Laboratory for Mechanical Behavior of Materials under Grant no. 20161808, the National Natural Science Foundation of China under Grant nos. 51402255 and 51872254, Yangzhou Science Fund for Distinguished Young Scholars under Grant no. YZ2017096. The authors also thank the Walloon Region of Belgium in the framework of the European FEDER project Micro+.

References

[1] J. Kang, J. Park, H. Lee, Pt-doped SnO_2 thin film based micro gas sensors with high selectivity to toluene and HCHO, Sens. Actuators B Chem. 248 (2017) 1011–1016.
[2] S. Yan, X. Liang, H. Song, S. Ma, Y. Lu, Synthesis of porous CeO_2-SnO_2 nanosheets gas sensors with enhanced sensitivity, Ceram. Int. 44 (2018) 358–363.
[3] L. Xiao, S. Xu, G. Yu, S. Liu, Efficient hierarchical mixed Pd/SnO_2 porous architecture deposited microheater for low power ethanol gas sensor, Sens. Actuators B Chem. 255 (2018) 2002–2010.
[4] X. Deng, L. Zhang, J. Guo, Q. Chen, J. Ma, ZnO enhanced NiO-based gas sensors towards ethanol, Mater. Res. Bull. 90 (2017) 170–174.
[5] M. Hassan, W. Khan, P. Mishra, S.S. Islam, A.H. Naqvi, Enhancement in alcohol vapor sensitivity of Cr doped ZnO gas sensor, Mater. Res. Bull. 93 (2017) 391–400.
[6] M. Poloju, N. Jayababu, M. Reddy, Improved gas sensing performance of Al doped ZnO/CuO nanocomposite based ammonia gas sensor, Mater. Sci. Eng. B 227 (2018) 61–67.
[7] J. Xiao, C. Song, W. Dong, C. Li, Y. Yin, Synthesis, characterization, and gas sensing properties of WO_3 nanoplates, Rare Met. Mater. Eng. 46 (2017) 1241–1244.
[8] Y. Yao, M. Yin, J. Yan, D. Yang, S. Liu, Controllable synthesis of Ag-WO_3 core-shell nanospheres for light-enhanced gas sensors, Sens. Actuators B Chem. 251 (2017) 583–589.
[9] H. Kim, J. Lee, Highly sensitive and selective gas sensors using p-type oxide semiconductors: overview, Sens. Actuators B Chem. 192 (2014) 607–627.
[10] E. Turgut, Ö. Çoban, S. Sarıtaş, S. Tüzemen, M. Yıldırım, E. Gür, Oxygen partial pressure effects on the RF sputtered p-type NiO hydrogen gas sensors, Appl. Surf. Sci. 435 (2018) 880–885.
[11] Z. Li, Supersensitive and superselective formaldehyde gas sensor based on NiO nanowires, Vacuum 143 (2017) 50–53.
[12] H. Gao, D. Wei, P. Lin, C. Liu, G. Lu, The design of excellent xylene gas sensor using Sn-doped NiO hierarchical nanostructure, Sens. Actuators B Chem. 253 (2017) 1152–1162.
[13] H. Chen, C. Hsiao, W. Chen, C. Chang, W. Liu, Characteristics of a Pt/NiO thin film-based ammonia gas sensor, Sens. Actuators B Chem. 256 (2018) 962–967.
[14] H. Gao, L. Zhao, L. Wang, P. Sun, G. Lu, Ultrasensitive and low detection limit of toluene gas sensor based on SnO_2-decorated NiO nanostructure, Sens. Actuators B Chem. 255 (2018) 3505–3515.
[15] J. Hu, J. Yang, W. Wang, Y. Xue, Y. Chen, Synthesis and gas sensing properties of NiO/SnO_2 hierarchical structures toward ppb-level acetone detection, Mater. Res. Bull. 102 (2018) 294–303.
[16] D. Lahem, R.L. Fomekong, J. N.i Lambi, A. Delcorte, L. Bilteryst, M. Gonon, M. Debliquy, Influence of synthesis route on the formaldehyde gas sensing properties of nickel oxide nanostructures, Int. J. Mod. Eng. Res. 7 (2017) 12–21.
[17] R.L. Fomekong, H.M.T. Kamta, J.N. Lambi, D. Lahem, P. Eloy, M. Debliquy, A. Delcorte, A sub-ppm level formaldehyde gas sensor based on Zn-doped NiO prepared by a co-precipitation route, J. Alloy. Compd. 731 (2018) 1188–1196.
[18] J. Zhang, X. Liu, G. Neri, N. Pinna, Nanostructured materials for room temperature gas sensors, Adv. Mater. 28 (2016) 795–831.
[19] S. Fan, A.K. Srivastava, V.P. Dravid, UV-activated room-temperature gas sensing mechanism of polycrystalline ZnO, Appl. Phys. Lett. 95 (2009) 142106.
[20] X. Geng, C. Zhang, M. Debliquy, Cadmium sulfide activated zinc oxide coatings deposited by liquid plasma spray for room temperature nitrogen dioxide detection under visible light illumination, Ceram. Int. 42 (2016) 4845–4852.
[21] X. Geng, J. You, C. Zhang, Microstructure and sensing properties of CdS-ZnO_{1-x} coatings deposited by liquid plasma spray and treated with hydrogen peroxide solution for nitrogen dioxide detection at room temperature, J. Alloy. Compd. 687 (2016) 286–293.
[22] X. Geng, C. Zhang, Y. Luo, M. Debliquy, Preparation and characterization of Cu_xO_{1-y}@$ZnO_{1-\alpha}$ nanocomposites for enhanced room-temperature NO_2 sensing applications, Appl. Surf. Sci. 401 (2017) 248–255.
[23] C. Zhang, X. Geng, H. Liao, C. Li, M. Debliquy, Room-temperature nitrogen-dioxide sensors based on ZnO_{1-x} coatings deposited by solution precursor plasma spray, Sens. Actuators B Chem. 242 (2017) 102–111.
[24] X. Chen, L. Liu, P.Y. Yu, S.S. Mao, Increasing solar absorption for photocatalysis with black hydrogenated titanium dioxide nanocrystals, Science 331 (2011) 746–749.
[25] Z. Xue, Z. Cheng, J. Xu, Q. Xiang, X. Wang, J. Xu, Controllable evolution of dual defect Zn_i and V_O associate-rich ZnO nanodishes with (0001) exposed facet and its multiple sensitization effect for ethanol detection, ACS Appl. Mater. Interfaces 9 (2017) 41559–41567.
[26] M.D. McCluskey, S.J. Jokela, Defects in ZnO, J. Appl. Phys. 106 (2009) 071101.
[27] C. Zhang, X. Geng, J. Li, Y. Luo, P. Lu, Role of oxygen vacancy in tuning of optical,

ARTICLE IN PRESS

electrical and NO_2 sensing properties of ZnO_{1-x} coatings at room temperature, Sens. Actuators B Chem. 248 (2017) 886–893.
[28] J. Xu, Z. Xue, N. Qin, Z. Cheng, Q. Xiang, The crystal facet-dependent gas sensing properties of ZnO nanosheets: experimental and computational study, Sens. Actuators B Chem. 242 (2017) 148–157.
[29] S. Dey, S. Bhattacharjee, M. Chaudhuri, R. Bose, S. Halder, C. Ghosh, Synthesis of pure nickel(III) oxide nanoparticles at room temperature for Cr(VI) ion removal, RSC Adv. 67 (2015) 1–25.
[30] N. DucHoa, P. Tong, C. ManhHung, N. Duy, N. Hieu, Urea mediated synthesis of Ni $(OH)_2$ nanowires and their conversion into NiO nanostructure for hydrogen gas-sensing application, Int. J. Hydrog. Energy 43 (2018) 9446–9453.
[31] T. Zhai, S. Xie, Y. Zhao, X. Sun, X. Lu, M. Yu, M. Xu, F. Xiao, Y. Tong, Controllable synthesis of hierarchical ZnO nanodisks for highly photocatalytic activity, CrystEngComm 14 (2012) 1850–1855.
[32] D. Kohl, Topical review: function and applications of gas sensors, J. Phys. D Appl. Phys. 34 (2001) 125–149.
[33] C. Zhang, A. Boudiba, P. Marco, R. Snyders, M. Olivier, M. Debliquy, Room temperature responses of visible-light illuminated WO_3 sensors to NO_2 in sub-ppm range, Sens. Actuators B Chem. 181 (2013) 395–401.
[34] S. Park, D. Lee, B. Kwak, H. Lee, S. Lee, B. Yoo, Synthesis of self-bridged ZnO nanowires and their humidity sensing properties, Sens. Actuators B Chem. 268 (2018) 293–298.
[35] M. Zhang, H. Zhang, L. Li, K. Tuokedaerhan, Z. Jia, Er-enhanced humidity sensing performance in black ZnO-based sensor, J. Alloy. Compd. 744 (2018) 364–369.
[36] L. Gao, Z. Cheng, Q. Xiang, Y. Zhang, J. Xu, Porous corundum-type In_2O_3 nanosheets: synthesis and NO_2 sensing properties, Sens. Actuators B Chem. 208 (2015) 436–443.
[37] W. An, X. Wu, X.C. Zeng, Adsorption of O_2, H_2, CO, NH_3, and NO_2 on ZnO nanotube: a density functional theory study, J. Phys. Chem. C. 112 (2008) 5747–5755.
[38] Y. Qin, Z. Ye, DFT study on interaction of NO_2 with the vacancy-defected WO_3 nanowires for gas-sensing, Sens. Actuators B Chem. 222 (2016) 499–507.